Journal of Materials Chemistry A

PAPER

View Article Online
View Journal | View Issue

Cite this: J. Mater. Chem. A, 2015, 3, 2741

Enhancement of photocatalytic performance *via* a P3HT-*g*-C_3N_4 heterojunction†

Xiaojuan Bai,[ab] Changpo Sun,[b] Songling Wu[b] and Yongfa Zhu*[a]

Received 12th September 2014
Accepted 11th December 2014

DOI: 10.1039/c4ta04779f

www.rsc.org/MaterialsA

P3HT-*g*-C_3N_4 photocatalysts with high activity have been fabricated by assembling p-type P3HT particles on n-type *g*-C_3N_4 nanoplates *via* a ball milling method. The photocatalytic activity of the P3HT-*g*-C_3N_4 photocatalysts for the degradation of MB was 2 times higher than that of pure *g*-C_3N_4. The formation of a heterojunction interface of P3HT-*g*-C_3N_4 photocatalysts enhanced the separation efficiency of photogenerated electron–hole pairs and resulted in the enhancement of photocatalytic performance. The potential difference in the heterojunction is the main driving force for efficient charge separation and transfer.

Introduction

Composites of carbon nanomaterials and conjugated polymers have been used extensively as active materials in environmental purification, organic photosynthesis, solar energy conversion and sustainable hydrogen production.[1] In principle, heterogeneous photocatalysis involves the generation, migration, and separation of charge carriers in light-excited semiconductors, in which the adsorbed substrates undergo redox reactions with the separated electrons and holes.[2,3] Metal-free polymeric semiconductors have recently been introduced as solar energy transducers and have gained great attention. However, the photocatalytic systems developed thus far have been restricted by low efficiency, mainly because of the fast recombination of photoinduced electron–hole pairs.[4,5] The creation of tight junctions between two semiconductors not only depends on the electronic structure of the semiconductors but also on material properties, such as electron affinity and work function.[3,6] Several kinds of photocatalytic heterojunctions have been developed by coupling different types of photocatalysts. For example, the combination of p-type or n-type semiconductors has been reported to create p–n and n–n photocatalytic systems.[7–10] Recently, a binary carbon nitride (*g*-C_3N_4) based on s-triazine networks as a metal-free n-type photocatalyst for hydrogen production and environmental purification has been introduced.[1,11–13] Poly-3-hexylthiophene (P3HT) has proven thus far to be one of the best choices for p-type donor materials in bulk heterojunctions, and its use in conjunction with *g*-C_3N_4 as the n-type acceptor material is considered a natural combination due to very good hole and electron mobilities in the two materials, respectively,[14] and the potentially ideal nanostructure of their distributed heterojunction provided effective phase separation at the nanoscale. P3HT is a p-type semiconductor with a band gap of 1.9–2.1 eV, higher hole carrier mobility ($10^{-4} \sim 10^{-3}$ cm^2 V^{-1} s^{-1}), dissolubility, processability and long-term stability.[15,16] As illustrated in Fig. S1,† once *g*-C_3N_4 and P3HT are integrated together, the band alignment between the two materials results in the formation of a Type-II heterojunction. The redistribution of electrons and holes between *g*-C_3N_4 and P3HT may greatly reduce the energy-wasteful e^-–h^+ recombination, thus improving the photocatalytic activity. In principle it should be possible to realize that the successful separation and the prolonged lifetime of e^-–h^+ pairs are beneficial for photocatalysis (Fig. S2†).

Although the previous studies provided important insight into the electrical, optical, and structural properties of P3HT-*g*-C_3N_4 blends,[16] the structure–activity relationship of P3HT-*g*-C_3N_4 composites can only be understood based on their activity trend and interface electronic structure at the molecular scale. This work suggests that two main factors contribute to the efficiency of charge transfer at the interface: the formation of a type-II heterojunction in the built-in field favors effective charge transfer ("electronic" factor), and the structure of the donor molecules at the interface, where the extended conjugation favors charge transfer analogous to the effect of crystalline regions in bulk polymers ("structural" factor). For the *g*-C_3N_4 molecular structure, there are some docking sites containing $-NH_2$ and –NH– groups on the surface which are formed through thermal condensation, and this may be modified by many methods used in the polymer processing and chemistry field.[17,18]

[a]Department of Chemistry, Beijing Key Laboratory for Analytical Methods and Instrumentation, Tsinghua University, Beijing, 100084, China. E-mail: zhuyf@tsinghua.edu.cn

[b]Academy of State Administration of Grain, No. 11 Baiwanzhuang Street, Beijing, 100037, China

† Electronic supplementary information (ESI) available: Schematic illustration of the organic heterojunction, charge separation and photocatalytic process, TEM, XPS, BET, DRS and cycle experimental data of the P3HT-*g*-C_3N_4 composite. See DOI: 10.1039/c4ta04779f

In this work, P3HT-g-C_3N_4 photocatalysts were fabricated by a ball milling method which is an effective way to synthesize materials in the polymer processing and chemistry field. Since the π-conjugation effect of the polymer plays a crucial role in charge transfer, we combined Raman spectroscopy with the FTIR method to investigate the nature of π-conjugation and its impact on the photocatalysis of P3HT-g-C_3N_4. The varying relative concentrations of P3HT-g-C_3N_4 are investigated and the π-conjugation effect is elucidated systematically. This work demonstrates that the photocatalytic activity of P3HT-g-C_3N_4 for degradation of MB was 2 times higher than that of pure g-C_3N_4 and the physical mixture of the P3HT–C_3N_4 sample, which could be ascribed to the high separation efficiency of photogenerated electrons and holes across the heterojunction interface of P3HT-g-C_3N_4 photocatalysts.

Experimental section

Materials

The P3HT sample was supplied by J&K Scientific Ltd and the average molecular weight is 30 000. Dicyandiamide was purchased from Sinopharm Chemical Reagent Corp, P. R. China. All other reagents used in this research were analytically pure and used without further purification. The bulk C_3N_4 photocatalysts were synthesized as described in a previous paper.[16] Dicyandiamide (3 g) (Aldrich, 99%) in an open crucible was heated in static air with a ramping rate of 2.3 °C min^{-1} to 550 °C where it was held for 4 h. The product was collected and ground into powder in an agate mortar for further characterization and performance measurements. It should be claimed that the widely used "g-C_3N_4" in the literature is actually non-stoichiometric. Here we use "g-C_3N_4" to describe the products just to keep consistent with the general usage.

Synthesis of P3HT-g-C_3N_4 samples

The typical P3HT-g-C_3N_4 composite photocatalysts were prepared as follows: the bulk g-C_3N_4 was mixed with different amounts of P3HT and then was ball milled certain times resulting in ultrafine burgundy powder (300 rps). The product was collected for further characterization and performance measurements. With different P3HT amounts loaded on g-C_3N_4, the color of the final products is different, which changes from light-burgundy to deep-burgundy. The P3HT-g-C_3N_4 photocatalysts with different P3HT ratios from 0.2 wt% to 5.0 wt% were prepared according to the above method. As a reference, 0.7 wt% P3HT–C_3N_4 mixture was prepared by finely grinding a certain amount of bulk g-C_3N_4 and P3HT, and then stirred mechanically at low speed and energy to form a uniform P3HT–C_3N_4 mixture. The annealed composite was obtained by calcination of the 0.7 wt% P3HT-g-C3N4 composite at 120 °C for 4 h, which was due to the fact that the optimum hole mobility of 10^{-3} cm^2 V^{-1} s^{-1} for P3HT can be achieved at 120 °C.

The g-C_3N_4 and P3HT-g-C_3N_4 electrodes were prepared as follows: 4 mg of the as-prepared photocatalyst was suspended in 2 mL of water to produce a slurry, which was then dip-coated onto a 2 cm × 4 cm indium-tin oxide (ITO) glass electrode. Electrodes were exposed to UV light for 10 h to eliminate ethanol and subsequently calcined at 200 °C for 8 h under N_2 flow (rate = 60 mL min^{-1}). All investigated electrodes were of similar thickness (0.8–1.0 μm).

Characterization

Transmission electron microscopy (TEM) images were obtained by using a JEOL JEM-2011F field emission transmission electron microscope with an accelerating voltage of 200 kV. To avoid electron beam-induced damage, a low-intensity beam was used for collecting selected area electron diffraction (SAED) patterns. X-Ray diffraction (XRD) patterns of the powders were recorded at room temperature by using a Bruker D8 Advance X-ray diffractometer. The diffuse reflectance absorption spectra (DRS) of the samples were recorded in the range of 250 to 800 nm using a Hitachi U-3010 spectrometer equipped with an integrated sphere attachment and $BaSO_4$ was used as a reference. Raman spectra were recorded on a microscopic confocal Raman spectrometer (Renishaw 1000 NR) with an excitation of 514.5 nm laser light. The room-temperature photoluminescence (PL) spectra of g-C_3N_4 and P3HT-g-C_3N_4 samples were investigated utilizing the Perkin-Elmer LS55 spectrophotometer equipped with a xenon (Xe) lamp with an excitation wavelength of 370 nm. Fourier transform infrared (FTIR) spectra were recorded using a Perkin-Elmer spectrometer in the frequency range of 4000–450 cm^{-1} with a resolution of 4 cm^{-1}. X-Ray photoelectron spectroscopy (XPS) was performed on a PHI 5300 ESCA system. The beam voltage was 3.0 kV, and the energy of the Ar ion beam was 1.0 keV. The binding energies were normalized to the signal for adventitious carbon at 284.8 eV. Electrochemical and photoelectrochemical measurements were performed in a three electrode quartz cell with 0.1 M Na_2SO_4 electrolyte solution. Platinum wire was used as the counter electrode and a saturated calomel electrode (SCE) was used as a reference electrode. g-C_3N_4 and P3HT-g-C_3N_4 film electrodes on ITO served as the working electrodes. The photoelectrochemical experimental results were recorded with an electrochemical system (CHI-660B, China). The visible irradiation was obtained from a 500 W Xe lamp (Institute for Electric Light Sources, Beijing) with a 420 nm cut-off filter. Potentials are given with reference to the SCE. The photoresponses of the photocatalysts to on/off visible light illumination were measured at 0.0 V.

Photocatalytic experiments

The photocatalytic activities were evaluated by the decomposition of methylene blue (MB) and phenol under visible light irradiation (λ > 420 nm). Visible irradiation was obtained from a 500 W Xe lamp (Institute for Electric Light Sources, Beijing) with a 420 nm cutoff filter, and the average visible light intensity was 38 mW cm^{-2}. 25 mg of the photocatalyst was totally dispersed in an aqueous solution of MB (50 mL, 0.03 mM) or phenol (50 mL, 5 ppm). Before irradiation, the suspensions were magnetically stirred in the dark for 60 min to achieve absorption–desorption equilibrium between the photocatalyst and MB (phenol). At certain time intervals, 3 mL aliquots were sampled and centrifuged to

remove the particles. The concentration of MB was analyzed by recording the absorbance at the characteristic band of 663 nm using a Hitachi U-3010 UV-vis spectrophotometer and phenol was detected using a HPLC method with a UV detector at 270 nm. To investigate the active species generated in the photocatalytic degradation process, the trapping experiments of free radicals (hydroxyl radical ($^{\bullet}OH$), hole (h^{+}), and superoxide radical capture) were carried out by using *tert*-butylalcohol (*t*BuOH), ethylenediamine tetraacetic acid disodium salt (EDTA-2Na) and benzoquinone, respectively.

Results and discussion

Morphology of P3HT-*g*-C_3N_4 photocatalysts

The successful formation of the P3HT-*g*-C_3N_4 heterostructure is clearly demonstrated by the TEM images in Fig. 1. The thin layers and regular spheres are identified for *g*-C_3N_4 and P3HT (Fig. 1a and the inset image), respectively. As shown in Fig. 1b, the *g*-C_3N_4 sample is found to be closely packed on the P3HT surface, exhibiting dense thick sheets, both of which are integrated together as a p–n heterojunction, resulting in the P3HT-*g*-C_3N_4 hybrid. The results revealed that P3HT adsorbs strongly to the *g*-C_3N_4 through stacking forces which formed various structures ranging from lamellar assemblies to more disordered, bundled conformations. It can be observed that the two phases of *g*-C_3N_4 and P3HT are in close contact to form an intimate interface. According to the previous reports and our experimental results[19–21] (Fig. S3†) the two-dimensional ordering of *g*-C_3N_4 and P3HT is very weak and it is hard to find the clear lattice fringe of *g*-C_3N_4 and P3HT from the high-resolution TEM image, which was attributed to the indistinct in-plane diffraction (100) in the XRD pattern.

These P3HT-*g*-C_3N_4 p–n heterostructures were further characterized by using the high-resolution X-ray photoelectron spectroscopy (XPS) spectra of S 2p and C 1s. In Fig. 1c, two independent binding energy (BE) peaks of S 2p centering at 162.7 eV and 163.8 eV are found for P3HT-*g*-C_3N_4, but are absent for the pristine *g*-C_3N_4. These BE values are close to those of the pristine P3HT (162.2 eV and 163.2 eV). Thus, the S 2p spectra of P3HT-*g*-C_3N_4 further confirm the formation of P3HT-*g*-C_3N_4 heterostructures. In addition, as shown in Fig. 1d, the BEs of C 1s for P3HT-*g*-C_3N_4 (283.7 eV and 287.0 eV) are quite different from those of pristine *g*-C_3N_4 (283.6 eV and 286.8 eV), illustrating that the grafted P3HT modified the *g*-C_3N_4, rather than providing a sulfur source for doping the *g*-C_3N_4 matrix by ball milling treatment at high energy. As shown in Fig. S4,† the N 1s intensity of P3HT-*g*-C_3N_4 composites shows the opposite tendency relative to S 2p and C 1s, and the C–N–C peak (398.8 eV) shifts slightly to the higher binding energy, illustrating that the P3HT nanospheres were wrapped chemically by *g*-C_3N_4 nanoplates.

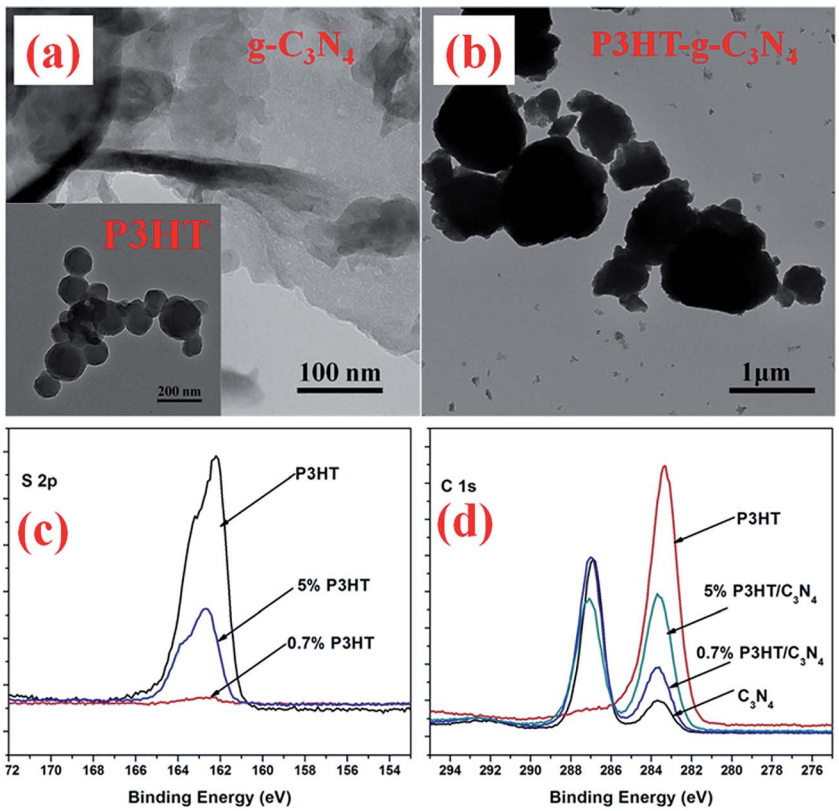

Fig. 1 (a) TEM images of *g*-C_3N_4 and P3HT (inset) semiconductor. (b) TEM image of the P3HT-*g*-C_3N_4 polymer composite. (c) High-resolution XPS spectra of S 2p recorded from P3HT, *g*-C_3N_4 and P3HT-*g*-C_3N_4. (d) High-resolution XPS spectra of C 1s.

Enhancement of photocatalytic activity

The rate of photodegradation of MB on P3HT-g-C_3N_4 photocatalysts with different amounts of P3HT is shown in Fig. 2a and b. With an increase in the amount of P3HT and the extended time, the rate of photodegradation of MB increases initially and then achieves a maximum when the amount of P3HT is about 0.7 wt% by ball milling treatment for 4 h. The apparent reaction rate is estimated to be as high as 0.18134 h^{-1} and the activity increased up to 2 times for a high concentration of MB after adding 0.7 wt% P3HT to g-C_3N_4. However, the rate of photodegradation of MB decreases when the amount of P3HT is higher than 0.7 wt%. The density of P3HT nanospheres wrapped by g-C_3N_4 nanoplates increases step-by-step with the enhancement of the P3HT content. In the case of the 0.7 wt% P3HT-g-C_3N_4 heterojunction, the surface of P3HT has been covered by g-C_3N_4 nanoplates well. However, further increase of the P3HT content results in a drastic overlapping of P3HT nanospheres, which is a drawback for fabrication of a heterojunction with a close interface. Only tight coupling is favorable for charge transfer between g-C_3N_4 and P3HT and promotes the separation of photogenerated electron–hole pairs, subsequently improving the photocatalytic activity. The P3HT-g-C_3N_4 sample also shows obviously higher photocatalytic activity for the decomposition of phenol than pristine g-C_3N_4 (Fig. 2c). After the annealing treatment, the photodegradation rate on P3HT-g-C_3N_4 decreases slightly, which may be induced by the change in the molecular arrangement during the annealing process (Fig. 2d). Fig. S5† illustrates the relationship between the degradation ratio of MB and cycle times. After reusing four cycles of about 20 h, the photodecomposition rate of 0.7 wt% P3HT-g-C_3N_4 for MB still remains over 80%.

Structure of heterojunction photocatalyst

The UV-visible diffuse reflectance spectra (DRS) show that the onset of the absorption edge of g-C_3N_4 is at 450 nm, corresponding to the band gap of 2.75 eV (shown in Fig. 3a). Furthermore, the absorption intensity of the P3HT-g-C_3N_4 composites increases remarkably with an increase in the amount of P3HT, and its edge could shift to 704 nm. Note that the physical mixture of P3HT and g-C_3N_4 failed to produce close interconnection between P3HT and g-C_3N_4 (Fig. S6†). X-Ray diffraction patterns (XRD) from the samples, shown in Fig. 3b, indicate that coupling C_3N_4 with P3HT can form intimate interfaces between C_3N_4 and P3HT in the P3HT-g-C_3N_4 heterojunction, rather than forming loose interfaces in the mechanically mixed sample. Raman spectroscopy is a simple and widely used technique to study the vibrational modes of molecules. This technique together with quantum chemical calculations of Raman modes can provide an important insight into the fundamental structure–property relationships of molecular materials.[22–24] Fig. 3c shows the typical Raman spectra of g-C_3N_4, P3HT and P3HT-g-C_3N_4 samples excited at 514 nm. g-C_3N_4 shows a weak Raman signal but there are various Raman modes at 400–2000 cm^{-1} for P3HT and P3HT-g-C_3N_4 samples: the main in-plane ring skeleton modes at ~1455 cm^{-1} (symmetric C=C stretching mode) and at ~1376 cm^{-1} (C–C intra-ring stretching mode), the inter-ring C–C stretching mode at ~1208 cm^{-1}, the C–H bending mode with the C–C inter-ring stretching mode at ~1180 cm^{-1}, and the C–S–C deformation mode at 728 cm^{-1}.[25,26] Among these Raman modes, we focus on the two main in-plane ring skeleton modes at ~1455 and ~1376 cm^{-1}, as they are supposed to be sensitive to the π-electron delocalization (conjugation length) of P3HT molecules.[27] The Raman intensity

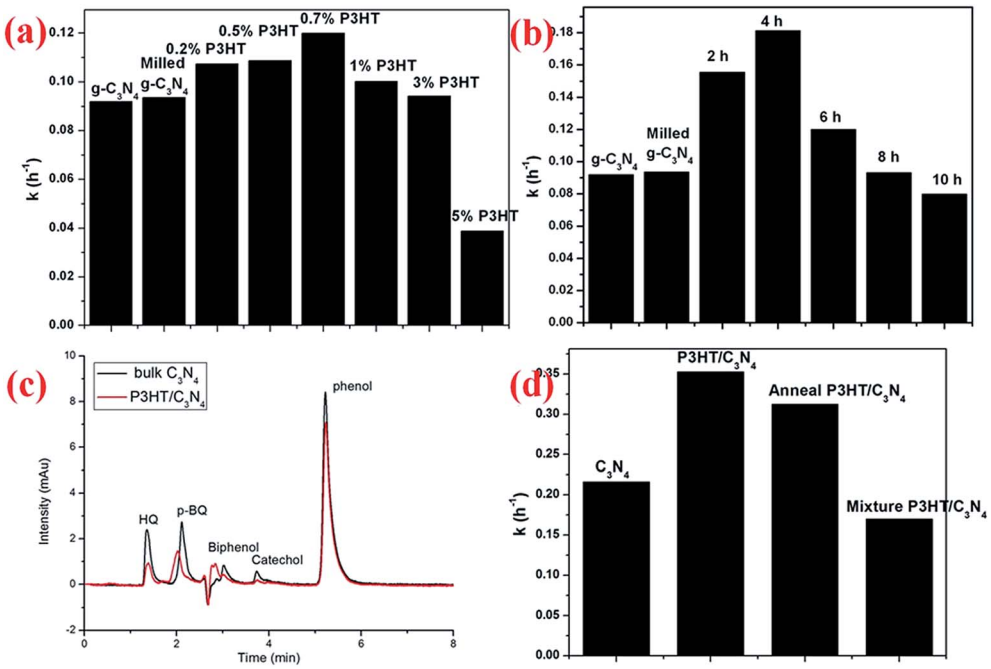

Fig. 2 (a) Apparent rate constants for the photocatalytic degradation of MB over the P3HT-g-C_3N_4 composite with different amounts of P3HT. (b) The rate of the degradation of MB over the P3HT-g-C_3N_4 composite for different ball-milling times. (c) The rate of degradation of phenol. (d) The rate of MB degradation on the mixture and annealed product. (visible light: $\lambda > 420$ nm, [MB] = 0.03 mM, [phenol] = 5 ppm).

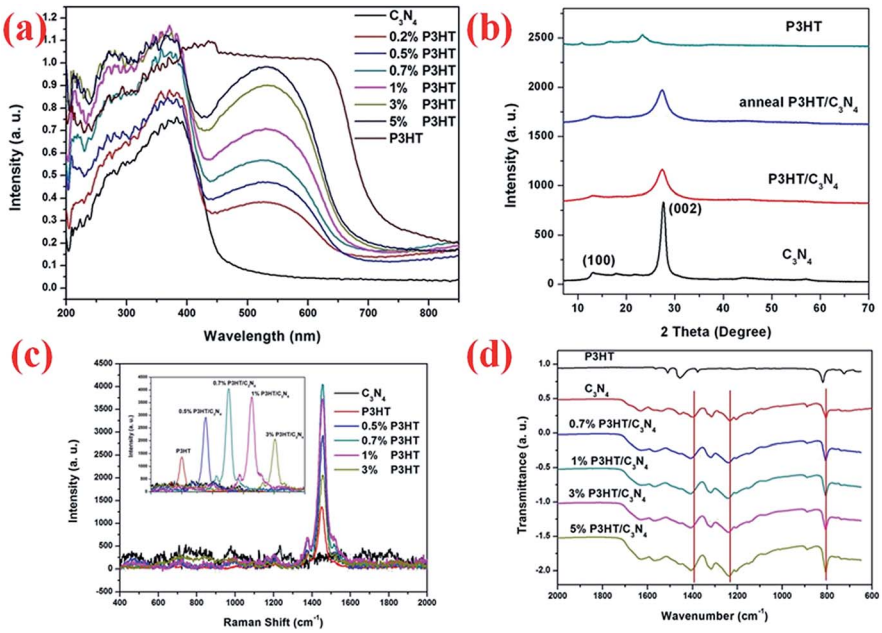

Fig. 3 (a) DRS of the P3HT-*g*-C_3N_4 polymer composite, (b) XRD patterns of the P3HT-*g*-C_3N_4 polymer composite, (c) Raman spectrum of the P3HT-*g*-C_3N_4 composite under 514 nm excitation and (d) FT-IR spectrum of the P3HT-*g*-C_3N_4 composite.

of the C=C mode for P3HT-*g*-C_3N_4 (0.7 wt%) under 514 nm excitation increased approximately 3-fold in comparison with pristine P3HT, which is induced by a pre-resonance Raman effect leading to an increase in the intensity of the Raman peaks, indicating that more ordered and longer conjugated segments exist in the P3HT-*g*-C_3N_4 system. According to a previous report, for P3HT, the intensity of the C–C mode relative to the C=C mode ($I_{C-C}/I_{C=C}$) decreases with decreasing chain length, without significant changes in the peak position.[28] This result suggests that a molecule with a shorter conjugation segment has a smaller relative C–C mode intensity as compared to a molecule with a longer conjugation segment. For the P3HT-*g*-C_3N_4 system, a shorter conjugation segment of P3HT means that a more widely conjugated system between P3HT and *g*-C_3N_4 is formed. It is worth noting that an interesting trend of the Raman intensity and photocatalysis exists in the P3HT-*g*-C_3N_4 system. The trend of such a change of the C=C mode peak intensity is consistent with the photocatalytic activity. The relationship between them may be attributed to a longer conjugated length with planar chain conformation than that of pristine *g*-C_3N_4, which is consistent with a higher degree of molecular ordering in P3HT-*g*-C_3N_4. This high degree of molecular order can lead to an increase in absorption at longer wavelength and a dramatic increase in hole carrier mobility as compared to its disordered form.[29–31] Therefore, the degree of molecular order of P3HT-*g*-C_3N_4 in the systems is well correlated with the performance of the photocatalytic activity. FTIR spectra are shown in Fig. 3d, the band at 1392 cm^{-1} of P3HT-*g*-C_3N_4 may be attributed to shifting of the characteristic vibrational band (1407 cm^{-1}) of *g*-C_3N_4 toward a shorter wavelength, suggesting that the chemical bonding effect in the π-conjugated system between P3HT and *g*-C_3N_4 is reinforced.

Mechanism of enhancement of photocatalytic activity

Photoluminescence (PL) spectra originating from the recombination of free charge carriers usually serve as a good candidate for the characterization of heterostructures, indicating the processes of charge migration, transfer and separation.[3,32,33] In Fig. 4a, a strong PL emission peak centered at 451 nm is observed for the pristine *g*-C_3N_4, which is attributed to the radiative recombination of charge carriers. This energy-wasteful process can be greatly suppressed in P3HT-*g*-C_3N_4 with the localization of electrons in *g*-C_3N_4 on one side and holes in P3HT on the other side by the band offsets. The formation rate of ˙OH at the photo-illuminated sample–water interface could also be detected by the PL technique using TA (terephthalic acid) as a probe molecule (Fig. 4b). The amount of ˙OH produced in the photo-irradiated P3HT-*g*-C_3N_4 suspension was estimated by measuring the amount of TAOH, which was generated by the reaction of ˙OH with TA. The fluorescence intensity increases with irradiation time under visible light irradiation. Thus, the intrinsic drawbacks of fast charge recombination in polymeric P3HT-*g*-C_3N_4 photocatalysts have been addressed by the construction of heterostructures, and a better photocatalytic performance has been realized. The BET surface area (S_{BET}) of the pure *g*-C_3N_4 and 5.0 wt% composites was 15.8 and 4.8 $m^2\ g^{-1}$, respectively, while that of 0.7 wt% composites was 3.8 $m^2\ g^{-1}$, which is lower than those of pure *g*-C_3N_4 and 5.0 wt% composites (Fig. S7†). This result demonstrated that the S_{BET} of the P3HT-*g*-C_3N_4 composite catalysts decreased with the addition of P3HT, indicating that the specific surface area does not contribute to the photocatalytic activity of composite photocatalysts.

To further confirm the mechanism, the trapping experiments of radicals were performed using *t*-BuOH as a hydroxyl

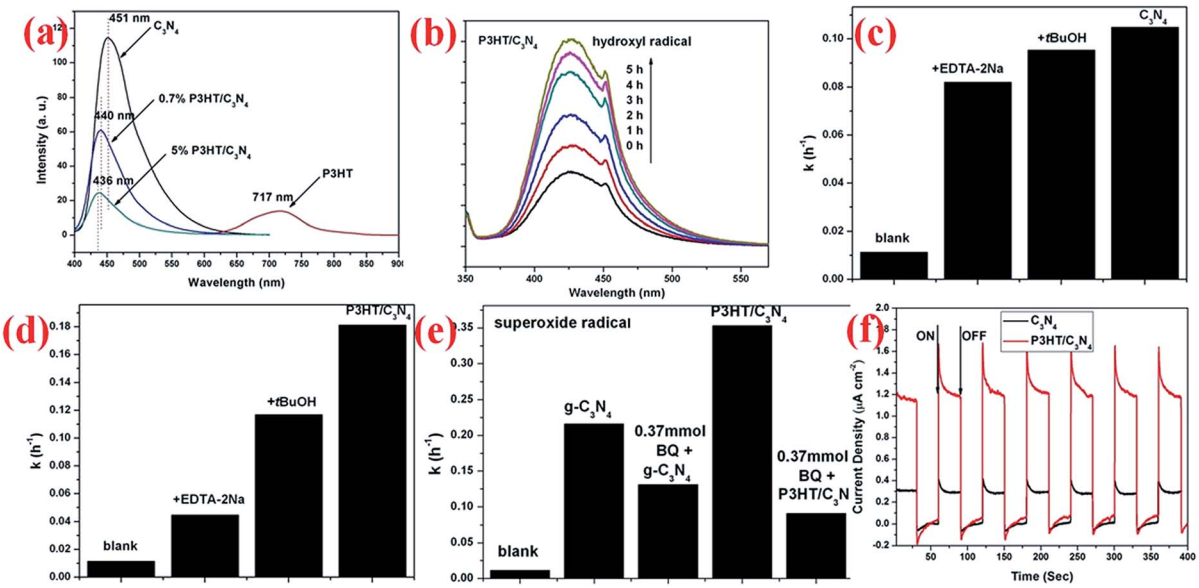

Fig. 4 (a) PL spectra of the P3HT-g-C_3N_4 polymer composite under 370 nm excitation at 298 K. (b) The changes in the fluorescence spectra of the irradiated P3HT-g-C_3N_4 (0.5 g L^{-1}) suspension containing 4 mM disodium terephthalate after various irradiation periods. (c) The rate of the degradation of MB over g-C_3N_4 with the addition of holes and a hydroxyl radical scavenger. (d) The rate of the degradation of MB over the P3HT-g-C_3N_4 composite with the addition of scavengers. (e) The rate of the degradation of MB with the addition of a superoxide radical scavenger over g-C_3N_4 and P3HT-g-C_3N_4. (f) The photocurrent generation at g-C_3N_4 and P3HT-g-C_3N_4 electrodes in 0.1 M Na_2SO_4 aqueous solution without any bias potential.

radical scavenger,[34] EDTA-2Na as a hole radical scavenger[35] and benzoquinone as a superoxide radical scavenger.[36] As shown in Fig. 4c–e, the photocatalytic activity of P3HT-g-C_3N_4 samples reduced largely accordingly, while the activity of g-C_3N_4 decreased slightly by the addition of the hole capture agent and superoxide radical scavenger, indicating that holes and superoxide radicals are the main oxidative species for P3HT-g-C_3N_4 samples, which is attributed to high hole carrier mobility of the longer conjugation segment of P3HT-g-C_3N_4. The photocurrent generation by the heterostructure was examined without any bias potential (Fig. 4f). Upon visible light irradiation, a fast and stable photocurrent was produced, indicating the generation and separation of photoinduced e^-–h^+ pairs at sample–water interfaces. As expected, an overall enhanced photocurrent is obtained on P3HT-g-C_3N_4, which may be attributed to the improved efficiency of charge separation and the prolonged lifetime of charge carriers involved in the photoredox reaction.

In summary, while g-C_3N_4 was hybridized by P3HT, a p–n heterojunction would be formed and the charge carriers would diffuse in the opposite direction to form an internal electric field in the direction from n-type g-C_3N_4 to p-type P3HT at the heterojunction interface. P3HT and g-C_3N_4 could be simultaneously excited to generate electron–hole pairs. According to the band edge position, the excited electrons produced by P3HT were injected into the CB of g-C_3N_4, while the photogenerated holes were effectively collected in the VB of P3HT. Because of the formation of the internal electric field, the migration of photogenerated carriers was promoted. Therefore, the photogenerated carriers could be effectively separated, resulting in higher photocatalytic performance.

Conclusions

P3HT-g-C_3N_4 heterojunctions were prepared by a blend method based on Type-II p–n junction band alignment between P3HT and g-C_3N_4. The enhancement of photocatalytic activity could be ascribed to the formation of an internal electric field induced by the enhanced separation efficiency of photogenerated electrons and holes. P3HT plays an important role in increasing the π-conjugation length in the system, which is an effect derived from the π–π stacking interaction at the interface between p-type P3HT donor and n-type g-C_3N_4 acceptor system. This work could open possibilities for improved preparation and activity of photocatalytic materials based on a π-conjugated polymer in general.

Acknowledgements

This work was partly supported by the National Basic Research Program of China (973 Program) (2013CB632403 and 2013CB127800), the National High Technology Research and Development Program of China (2012AA062701) and the Chinese National Science Foundation (21437003 and 21373121).

Notes and references

1 X. C. Wang, K. Maeda, A. Thomas, K. Takanabe, G. Xin, K. Domen and M. Antonietti, *Nat. Mater.*, 2009, **8**, 76.
2 K. Maeda, A. Xiong, T. Yoshinaga, T. Ikeda, N. Sakamoto, T. Hisatomi, M. Takashima, D. Lu, M. Kanehara,

T. Setoyama, T. Teranishi and K. Domen, *Angew. Chem., Int. Ed.*, 2010, **49**, 4096.
3 J. S. Zhang, M. W. Zhang, R. Q. Sun and X. C. Wang, *Angew. Chem.*, 2012, **124**, 10292.
4 M. Schwab, M. Hamburger, X. Feng, J. Shu, H. Spiess, X. Wang, M. Antonietti and K. Mullen, *Chem. Commun.*, 2010, **46**, 8932.
5 K. Maeda and K. Domen, *J. Phys. Chem. Lett.*, 2010, **1**, 2655.
6 J. Tersoff, *Phys. Rev. B: Condens. Matter Mater. Phys.*, 1984, **30**, 4874.
7 G. Li and K. A. Gray, *Chem. Phys.*, 2007, **339**, 173.
8 H. G. Kim, P. H. Borse, J. S. Jang, E. D. Jeong and J. S. Lee, *Mater. Lett.*, 2008, **62**, 1427.
9 X. P. Lin, J. C. Xing, W. D. Wang, Z. C. Shan, F. F. Xu and F. Q. Huang, *J. Phys. Chem. C*, 2007, **111**, 18288.
10 O. Khaselev and J. A. Turner, *Science*, 1998, **280**, 425.
11 X. Wang, K. Maeda, X. Chen, K. Takanabe, K. Domen, Y. Hou, X. Fu and M. Antonietti, *J. Am. Chem. Soc.*, 2009, **131**, 1680.
12 J. Zhang, M. Grzelczak, Y. Hou, K. Maeda, K. Domen, X. Fu, M. Antonietti and X. Wang, *Chem. Sci.*, 2012, **3**, 443.
13 X. J. Bai, L. Wang, R. L. Zong and Y. F. Zhu, *J. Phys. Chem. C*, 2013, **117**, 9952.
14 A. C. Mayer, S. R. Scully, B. E. Hardin, M. W. Rowell and M. D. McGehee, *Mater. Today*, 2007, **10**, 28.
15 B. R. Saunders and M. L. Turner, *Adv. Colloid Interface Sci.*, 2008, **138**, 1.
16 H. J. Yan and Y. Huang, *Chem. Commun.*, 2011, **47**, 4168.
17 J. Zhang, G. Zhang, X. Chen, S. Lin, L. Mohlmann, G. Dolega, G. Lipner, M. Antonietti, S. Blechert and X. Wang, *Angew. Chem.*, 2012, **124**, 3237.
18 J. Zhang, M. Zhang, G. Zhang and X. Wang, *ACS Catal.*, 2012, **2**, 940.
19 F. Dong, Z. W. Zhao, T. Xiong, Z. L. Ni, W. D. Zhang, Y. J. Sun and W. K. Ho, *ACS Appl. Mater. Interfaces*, 2013, **5**, 11392.
20 Y. L. Tian, B. B. Chang, J. L. Lu, J. Fu, F. N. Xi and X. P. Dong, *ACS Appl. Mater. Interfaces*, 2013, **5**, 7079.
21 X. J. Bai, R. L. Zong, C. X. Li, D. Liu, Y. F. Liu and Y. F. Zhu, *Appl. Catal., B*, 2014, **147**, 82.
22 E. C. Honea, A. Ogura, C. A. Murray, K. Raghavachari, Wo. Sprenger, M. F. Jarrold and W. L. Brown, *Nature*, 1993, **366**, 42.
23 C. L. Donley, J. Zaumseil, J. W. Andreasen, M. M. Nielsen, H. Sirringhaus, R. H. Friend and J. S. Kim, *J. Am. Chem. Soc.*, 2005, **127**, 12890.
24 J. P. Schmidtke, J. S. Kim, J. Gierschner, C. Silva and R. H. Friend, *Phys. Rev. Lett.*, 2007, **99**, 167401.
25 M. Baibarac, M. Lapkowski, A. Pron, S. Lefrant and I. Baltog, *J. Raman Spectrosc.*, 1998, **29**, 825.
26 A. M. Ballantyne, T. A. M. Ferenczi, M. Campoy-Quiles, T. M. Clarke, A. Maurano, K. H. Wong, W. M. Zhang, N. Stingelin-Stutzmann, J. S. Kim, D. D. C. Bradley, J. R. Durrant, I. McCulloch, M. Heeney, J. Nelson, S. Tierney, W. Duffy, C. Mueller and P. Smith, *Macromolecules*, 2010, **43**, 1169.
27 Y. Gao and J. K. Gery, *J. Am. Chem. Soc.*, 2009, **131**, 9654.
28 W. C. Tsoi, D. T. James, J. S. Kim, P. G. Nicholson, C. E. Murphy, D. D. C. Bradley, J. Nelson and J. S. Kim, *J. Am. Chem. Soc.*, 2011, **133**, 9834.
29 P. J. Brown, D. S. Thomas, A. Kohler, J. S. Wilson, J. S. Kim, C. M. Ramsdale, H. Sirringhaus and R. H. Friend, *Phys. Rev. B: Condens. Matter Mater. Phys.*, 2003, **67**, 064203.
30 S. S. Pandey, W. Takashima, S. Nagamatsu, T. Endo, M. Rikukawa and K. Kaneto, *Jpn. J. Appl. Phys., Part 2*, 2000, **39**, L94.
31 H. Sirringhaus, P. J. Brown, R. H. Friend, M. M. Nielsen, K. Bechgaard, B. M. W. Langeveld-Voss, A. J. H. Spiering, R. A. J. Janssen, E. W. Meijer, P. Herwig and D. M. de Leeuw, *Nature*, 1999, **401**, 685.
32 X. Gao, W. Sun, Z. Hu, G. Ai, Y. Zhang, S. Feng, F. Li and L. Peng, *J. Phys. Chem. C*, 2009, **113**, 20481.
33 T. Kawahara, Y. Konishi, H. Tada, N. Tohge, J. Nishii and S. Ito, *Angew. Chem.*, 2002, **114**, 2935.
34 H. Lee and W. Y. Choi, *Environ. Sci. Technol.*, 2002, **36**, 3872.
35 J. H. Zhou, C. Y. Deng, S. H. Si, Y. Shi and X. L. Zhao, *Electrochim. Acta*, 2011, **56**, 2062.
36 W. Liu, M. L. Wang, C. X. Xu and S. F. Chen, *Chem. Eng. J.*, 2012, **209**, 386.